Nanowires of conjugated polymer prepared by tuning the interaction between the solvent and polymer

Liang Chen [a, b], Kefeng Zhao [a, b], Xinxiu Cao [a, b], Jiangang Liu [a, *], Xinhong Yu [a], Yanchun Han [a, **]

[a] State Key Laboratory of Polymer Physics and Chemistry, Changchun Institute of Applied Chemistry, Chinese Academy of Sciences, 5625 Renmin Street, Changchun, 130022, PR China
[b] University of the Chinese Academy of Sciences, No.19A Yuquan Road, Beijing, 100049, PR China

ARTICLE INFO

ABSTRACT

The nanowire of conjugated polymer with higher density is desirable for its improved charge transport. However, at a higher solution concentration, the conjugated polymer chain entanglement is severe and not beneficial for the nucleation to grow nanowires. In this paper, we control the equilibrium of entanglement $\leftrightarrow$ disentanglement $\leftrightarrow$ nucleation and growth by tuning the radius of interaction (Ra) between the solvent and conjugated polymer. At the critical Ra, the disentangled polymer chain could nucleate to form nanowires because its content is moderately supersaturated. Thus, the equilibrium of entanglement $\leftrightarrow$ disentanglement is broken and the entangled polymer chain is further continuously disentangled to provide easier diffusivity of chains for nanowire formation. Accordingly, the dense nanowires of poly[2,5-bis(3-tetradecylthiophen-2-yl)thieno-[3,2-b]thiophene] (PBTTT-C14) were formed in the mixed solvent carbon disulfide (CS_2): cyclohexylbenzene (ChB) = 3:7 (Ra = 2.56) at a higher concentration of 1 mg/ml by aging. The density of the nanowire increased with increasing concentration and aging time. The nanowires were more than 10 μm in length and about 20 nm in width. The contrast was obvious in transmission electron microscopy which indicated the high electronic density and the high crystallinity of the nanowires.

© 2018 Published by Elsevier Ltd.

1. Introduction

Conjugated polymers have been extensively researched due to their good electronic properties and solution processing advantages in field-effect transistor (FET) and solar cells [1–5]. The charge transport in conjugated polymer thin films is influenced by the condensed matter such as molecular planarity, π-π stacking distance, crystallinity and long range order [6–11]. High crystallinity conjugated polymer nanowires provide the high long-range order of polymer chains and higher field-effect carrier transport [12–14].

The formation of nanowires in solution is generally considered to go through nucleation and growth process. The essential driving force for crystallization from solution relies on the degree of supersaturation. Conjugated polymer nanowires can be prepared by solubility difference, such as self-seeding method by changing the solution temperature [15–17], whisker method by aging the solution at selected solvent and temperature [18–21] and solvent slow evaporation [22–24]. The length of these nanowires was 10–100 μm and the width was more than 100 nm.

Although many kinds of conjugated polymer nanowires have been prepared successfully at special solvent and temperature, the general principle for choosing solvent to prepare the nanowire in solution with higher density needs further investigate. At a higher concentration, the solution becomes further supersaturated, where nucleation dominates crystal growth, and most of the excess solute becomes subject to spontaneous nucleation which is not beneficial for the growth of nanowires.

Conjugated polymer chain aggregation in solution prior to film fabrication is critical for their film structure. Solubility parameters are certain measurable quantities that are observed to influence the ability of a solvent to dissolve a polymer. The solvent selection principle of disentanglement could be proposed based on the Hansen solubility parameter and the radius of interaction (Ra)

---

between the solvent and polymer. Ra is defined as the distance between the solvent and polymer solubility parameter in Hansen space, by the following equation:

$$(Ra)^2 = 4(\delta_{D2} - \delta_{D1})^2 + (\delta_{P2} - \delta_{P1})^2 + (\delta_{H2} - \delta_{H1})^2 \quad (1)$$

where δ_{D2}, δ_{P2} and δ_{H2} are the Hansen parameters of the solvent, δ_{D1}, δ_{P1} and δ_{H1} are the Hansen parameters of the polymer. The Ra could tune the solubility and supersaturation. The solubility is increased to facilitate disentanglement with decreasing Ra. The supersaturation is the driving force of crystallization and could control the nucleation rate and growth rate. The aggregation of polymer could be governed by solubility parameter [25–31]. According to the solvent selection principle, the nanowires could be prepared in non-chlorinated solvents [32], this could avoid the use of chlorinated solvents in current literature.

Chain entanglements inhibit chain conformational changes and thus nucleation and growth process in conditions where the solution approaches its solubility limit. The entanglement and disentangled molecules were coexistent in solution [33]. In this work, we control the equilibrium of entanglement ↔ disentanglement ↔ nucleation and growth by tuning the radius of interaction (Ra) between the solvent and conjugated polymer. When the solution was at the critical Ra of 2.56, the entanglement was disentangled at higher concentration. The disentangled molecules could pack to nanowires which could facilitate the continuous disentanglement to grow dense nanowires at higher concentration. The dense nanowires of PBTTT-C14 were formed at the critical Ra and a higher concentration of 1 mg/ml by aging. The nanowires were more than 10 μm in length and 20 nm in width. The contrast was obvious in transmission electron microscopy which indicated the high electronic density and the high crystallinity of the nanowires. The density of the nanowire increased with increasing concentration and aging time.

2. Experimental

2.1. Materials

Poly[2,5-bis(3-tetradecylthiophen-2-yl)thieno-[3,2-b]thiophene] (PBTTT-C14) ($M_n = 28$ k, PDI = 1.8) was purchased from 1-Material Inc. and its structure is shown in Fig. 1. The solvent carbon disulfide (CS$_2$) was purchased from Beijing Chemical, China and cyclohexylbenzene (ChB) was purchased from Sigma-Aldrich Co. The solubility parameter of PBTTT-C14, CS$_2$ and ChB in Hansen space were shown in Fig. 1. The glass slides as substrates were cleaned in piranha solution (70/30 v/v of concentrated H$_2$SO$_4$ and 30% H$_2$O$_2$) at 90 °C for 20 min and then rinsed with deionized water and finally blown dry by nitrogen.

2.2. Sample preparation

The solvent with different Ra was prepared by mixing the CS$_2$ and ChB. The solution of the PBTTT-C14 with different Ra was dissolved at a concentration of 1 mg/ml and aged 36 h. The solution of different concentration was prepared in mixed solvent (CS$_2$: ChB = 3:7) and aged 36 h. The solution of different aged time was prepared at a concentration of 1 mg/ml in mixed solvent (CS$_2$: ChB = 3:7).

2.3. Characterization

The UV-Vis-NIR absorption spectra were recorded by using an AvaSpect-3648 optical fiber spectrometer.

Raman spectra were obtained with a LabRam HR800 spectrometer (Horiba Jobin Yvon) equipped with an Olympus BX41 microscope in the backscattering geometry. A 532 nm laser was focused on the sample with a 50× objective lens.

The films for transmission electron microscopy (TEM) characterization were made by drop-casting the solutions onto a copper grid. TEM images were obtained with a JEOL JEM-1011 transmission electron microscope operated at an accelerating voltage of 100 kV.

To fabricate organic field effect transistors (OFET) devices, highly doped n-type Si wafers with a 300 nm thermally grown oxide layer were used as the substrates. The gold source–drain electrodes were deposited by thermal evaporation in high vacuum (~4 × 10^{-4} Pa) to finish the preparation of OFETs. I-V curves were measured to characterize the performances of OFETs. Field-effect characteristic measurements were carried out on a Keithley 4200 semiconductor parameter analyzer under ambient conditions. The charge-carrier mobility was calculated using the formula:

$$\mu = \frac{2L}{WC_i}\left(\frac{\partial\sqrt{I_{SD}}}{\partial V_G}\right)^2 \quad (2)$$

where L = 0.2 mm, W = 6 mm, C$_i$ = 10 nF/cm^2.
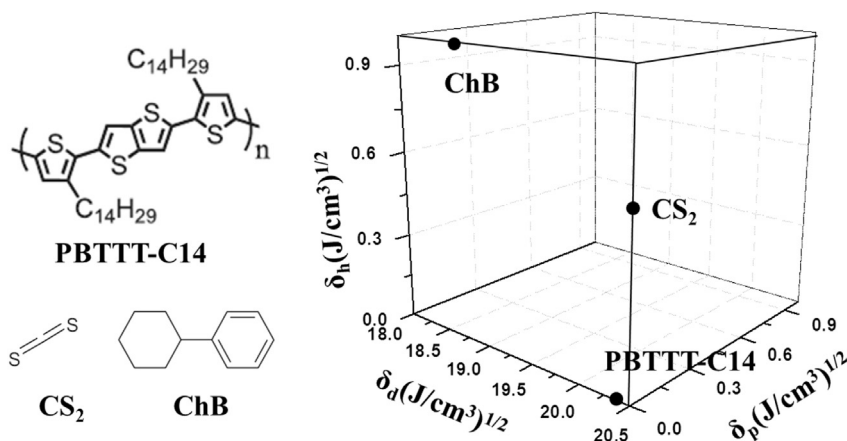
Fig. 1. The chemical structure of the PBTTT-C14, CS$_2$ and ChB. The solubility parameter is shown in Hansen space.

3. Results and discussion

3.1. Preparing nanowires in critical Ra solution by disentanglement for nucleation

The free energy of mixing approach is more appropriate to explain the formation of nanowires. The Ra could represent the ΔG_M for dissolving the polymer in different mixed solvent of CS_2 and ChB.

The free energy of mixing is calculated by the following equation:

$$\Delta G_M = \Delta H_M - T\Delta S_M \qquad (3)$$

The ΔS_M is similar for dissolving the polymer in different mixed solvent of CS_2 and ChB due to the concentration is low (1 mg/ml).

The main difference of ΔG_M for dissolving the polymer in different mixed solvent is the ΔH_M.

$$\Delta H_M = \varphi_1 \varphi_2 \left[(\delta_{D2} - \delta_{D1})^2 + (\delta_{P2} - \delta_{P1})^2 + (\delta_{H2} - \delta_{H1})^2 \right] \qquad (4)$$

The ΔG_M is decreased with decreasing the ΔH_M. The ΔH_M is decreased with decreasing the Ra according to equation (1). The Ra could represent the ΔG_M for dissolving the polymer in different mixed solvent of CS_2 and ChB.

The PBTTT-C14 nanowires were prepared by tuning the radius of interaction (Ra) between the solvent and polymer with mixed solvent of CS_2 and ChB. The solubility parameter of solvent and polymer was shown in Table 1. The solubility parameter of PBTTT-C14 was calculated by the group contribution. The solubility parameter of CS_2 and ChB was found from the handbook. The solubility parameter of the mixed solvent of CS_2 and ChB was calculated by the following equation:

$$\delta_M = \varphi_1 \times \delta_1 + \varphi_2 \times \delta_2 \qquad (5)$$

The Ra was calculated according to the solubility parameter of PBTTT-C14 and the mixed solvent of CS_2 and ChB, as shown in Table 2. The Ra was increased with increasing the ratio of ChB. The conformation and aggregation of the conjugated polymer in different mixed solvent was characterized by the UV-Vis-NIR absorption spectra and Raman spectra, as shown in Fig. 2. The max absorption peak was red-shifted from 480 nm to 530 nm with increasing Ra which indicated the longer conjugated length [34–36]. The peak at 590 nm indicated the π-π stacking and the intensity was increased with increasing Ra which indicated the molecules were aggregated. In the solvent with low Ra (such as Ra<2), the molecules were dissolved better and the solution didn't reach the saturation which couldn't result in π-π stacking and aggregation peak. In the solvent with high Ra, the solubility was decreased and the solution achieved the supersaturation. The aggregation was enhanced and the conjugated length was increased. The tendency of aggregation was stronger and the rate of aggregation was accelerated with increasing Ra. The growth of nanowires was a slow process to avoid the defect which would suppress crystallization and decrease the length of nanowires. The rapid aggregation in the solution with too high Ra would form many

Table 1
The solubility parameter of the conjugated polymer and solvent.

	$\delta_d (J/cm^3)^{1/2}$	$\delta_p (J/cm^3)^{1/2}$	$\delta_h (J/cm^3)^{1/2}$
PBTTT-C14	20.4	0	0
CS_2	20.5	0	0.6
ChB	18.7	0	1.0

Table 2
The radius of interaction (Ra) between the solvent and polymer of PBTTT-C14.

CS_2: ChB	10:0	9:1	5:5	3:7	1:9	0:10
Ra	0.63	0.63	1.79	2.56	3.16	3.54
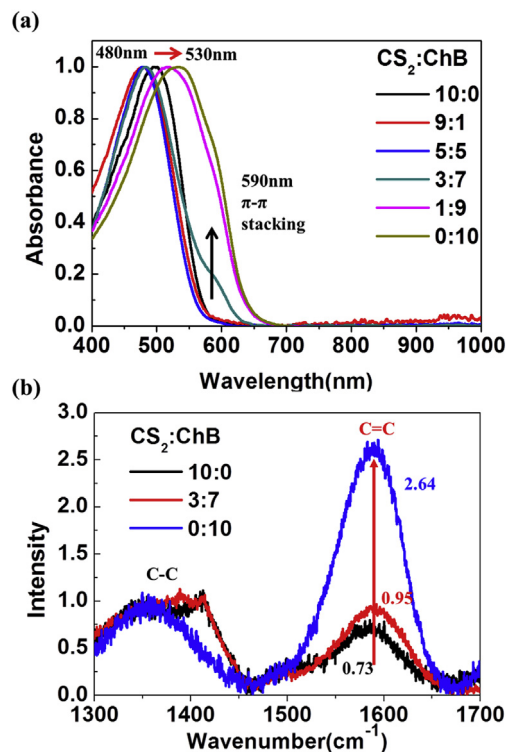
Fig. 2. (a) The UV-Vis-NIR absorption spectra for the solutions with different Ra. (b) The Raman spectra for the different Ra.

small crystals with defect. The molecules were entangled into the small crystals and couldn't move to the crystal front to form nanowires. The Raman spectra for the different Ra are shown in Fig. 2b. The intensity of the C=C stretching normalized by the intensity of the C-C feature was increased with increasing Ra which indicated the better electronic delocalization and conjugated length.

We need to investigate the morphology of the films drop-casting from the solution with different Ra and the requirement of Ra for forming nanowires.

The morphology of the films drop-casting from the solutions with different Ra was characterized, as shown in Fig. 3. The film drop-casting from CS_2 was featureless morphology. There were a few short nanowires in the film drop-casting from the mixed solvent (CS_2: ChB = 9:1), although the Ra was similar to CS_2. The different morphology at the same Ra was due to the difference in the film formation process. According to absorption spectra, there was no aggregation in the two kinds of solutions. The boiling point of ChB was higher than CS_2 (238 °C for ChB and 46 °C for CS_2). The time of film formation was longer for the mixed solvent than the film of CS_2. The short nanowires were formed during drop-casting from the mixed solvent. However the time of forming nanowires during the film formation was shorter than the time of forming nanowires in solution which resulted in the nanowires was short. The morphology obtained from the mixed solvent (Ra = 1.79) was also short nanowires. The dense and long nanowires were prepared when Ra was 2.56. The nanowires were more than 10 μm in length
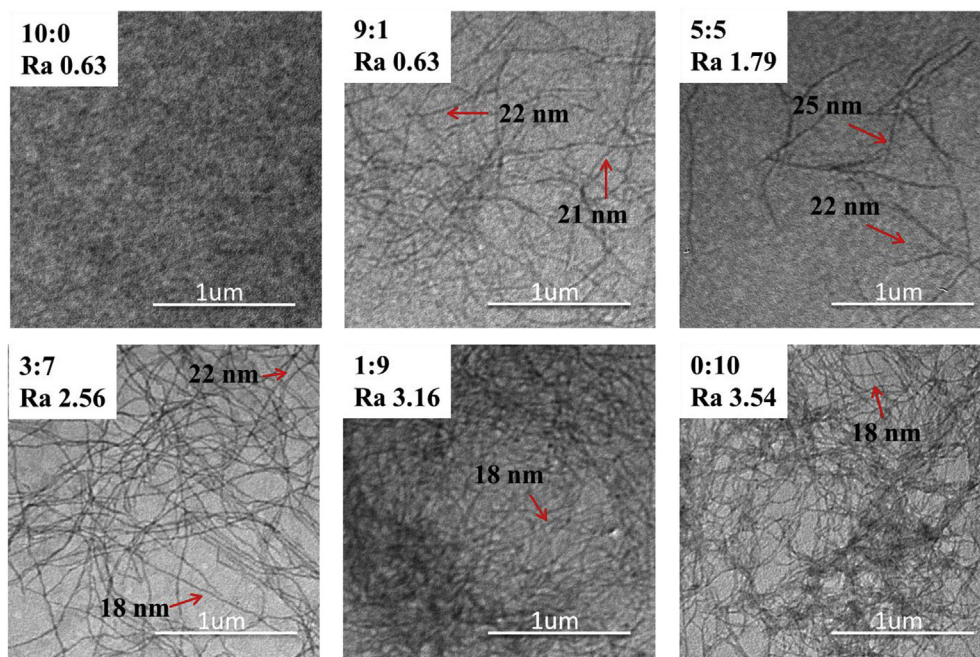
Fig. 3. The morphology of the films drop-casting from the solutions with different Ra.

and 20 nm in width. The contrast was obvious in transmission electron microscopy which indicated the high electronic density and the high crystallinity of the nanowires. According to absorption spectra, the aggregation was first formed in solution with increasing Ra to 2.56. This Ra was the critical value of aggregation. The supersaturation was the lowest and the molecules were disentangled at this Ra resulting in more ordered crystal nuclei because the perfect crystal nuclei was more stable in thermodynamics and couldn't be dissolved. The ordered crystal nuclei could grow to long nanowires and the growth in solution was slow to avoid the defect. The disentangled molecules could pack to nanowires which could facilitate the continuous disentanglement to grow dense nanowires at higher concentration. When the Ra was increased further, the amorphous aggregation was appeared. The tendency of aggregation was stronger and the rate of aggregation was accelerated in high Ra. When Ra is higher than the critical value, the entangled molecules couldn't grow nanowires. There were too many small crystals and the molecules were entangled into the small crystals which resulted in the amorphous aggregation. The equilibrium of entanglement ↔ disentanglement ↔ nucleation and growth could be controlled by tuning the Ra. The long nanowires were prepared when the Ra could achieve the critical value of the disentanglement.

The conjugated polymer nanowire with higher density promotes charge transport. The typical characteristic transfer curve of OFET was shown in Fig. 4. The field effect charge-carrier mobility of the film with long nanowires was increased from 9.6×10^{-4} $cm^2V^{-1}s^{-1}(CS_2)$ and 2.5×10^{-4} $cm^2V^{-1}s^{-1}(ChB)$ to 1.9×10^{-3} $cm^2V^{-1}s^{-1}$.

3.2. Tuning density of nanowires by changing concentration to control growth

The density of nanowires could be controlled by adjusting the concentration of the solution. The UV-Vis-NIR absorption spectra for the solutions with different concentration were characterized in Fig. 5. The max absorption peak was red-shifted from 470 nm to
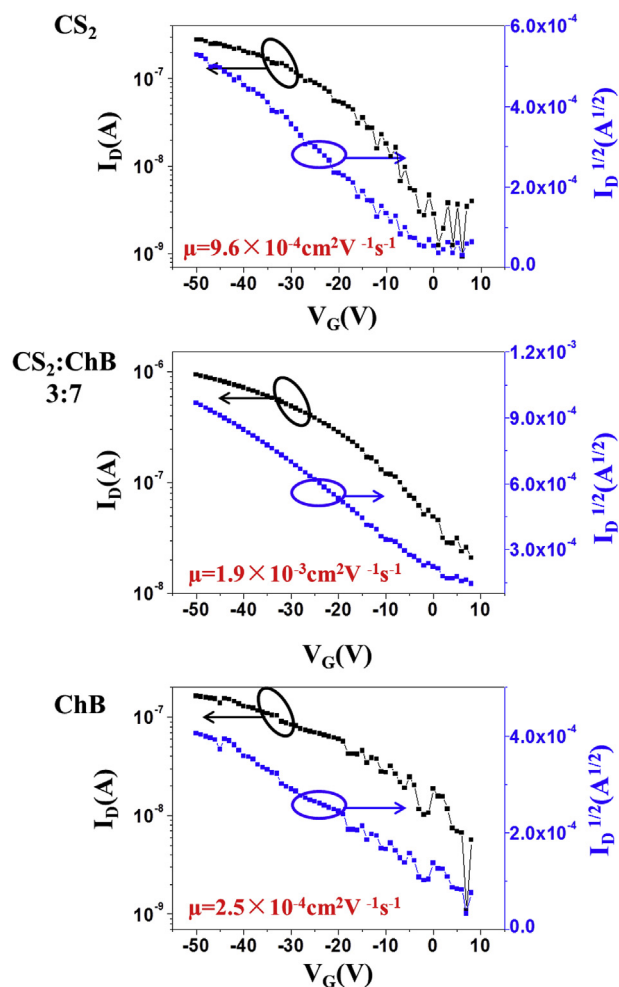
Fig. 4. The typical characteristic transfer curve of OFET.
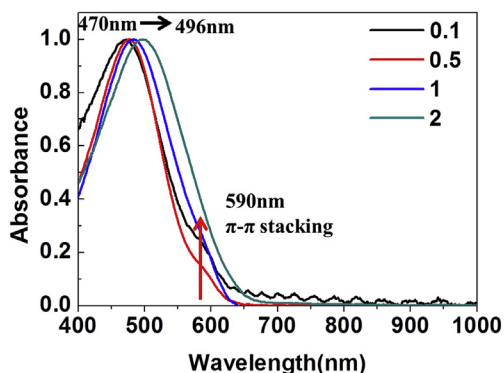
Fig. 5. The UV-Vis-NIR absorption spectra for the solutions with different concentration.

Fig. 7. The UV-Vis-NIR absorption spectra for the solutions with different aging time.

596 nm with increasing concentration which indicated the longer conjugated length. The peak at 590 nm indicated the π-π stacking and the intensity was increased with increasing concentration which indicated the molecules were aggregated. In the solution at low concentration, there were a few molecules to aggregate and the intensity of the π-π stacking absorption peak was weak. The aggregation was enhanced when there were more molecules with increasing concentration. The long and dense nanomires could be prepared when there were enough molecules to crystallize. However, the high concentration could lead to entanglement when the aggregation peak was enhanced which would suppress the nanomires formation. We would characterize the morphology of the films drop-casting from the solution at different concentration and investigate the requirement of concentration for forming dense nanowires.

The morphology of the films drop-casting from the solutions with different concentration was characterized, as shown in Fig. 6. There were a few short nanowires in the solution at the concentration of 0.1 mg/ml. The density of nanowires was increased and the length of nanowires was extended when the concentration was increased. There were dense and long nanowires at the concentration of 1 mg/ml. However the amorphous aggregation was appeared when the concentration was 2 mg/ml. The probability of
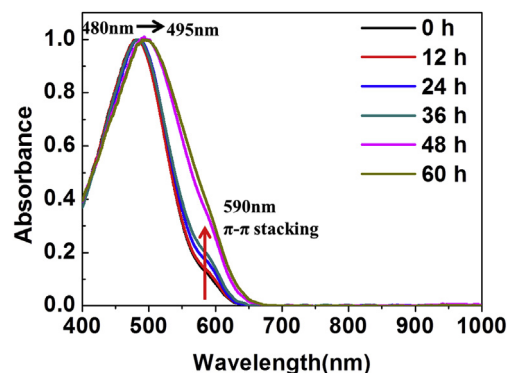
aggregation was increased with increasing concentration. There were a few molecules to form crystal nuclei at low concentration. The amount of crystal nuclei was small which resulted in the density of nanowires was low. There were not enough molecules that could move to the crystal front to grow long nanowires at low concentration. When the concentration was increased, the amount of crystal nuclei was increased and there were more molecules to grow into the nanowires. The nanowires could become long and dense. The entanglement was severe when the concentration was too high. The entanglement would suppress the molecules move to the crystal front to form nanowires and form small crystal or amorphous aggregation. The density of nanowires could be tuned by changing concentration to influence the amount of crystal nuclei and crystal growth.

3.3. The formation process and crystallization mechanism of the nanowires

The formation process of the nanowires was characterized to investigate the crystallization mechanism. The UV-Vis-NIR absorption spectra for the solutions aging different time were characterized in Fig. 7. The max absorption peak was red-shifted from 480 nm to 495 nm and the intensity of the π-π stacking peak was
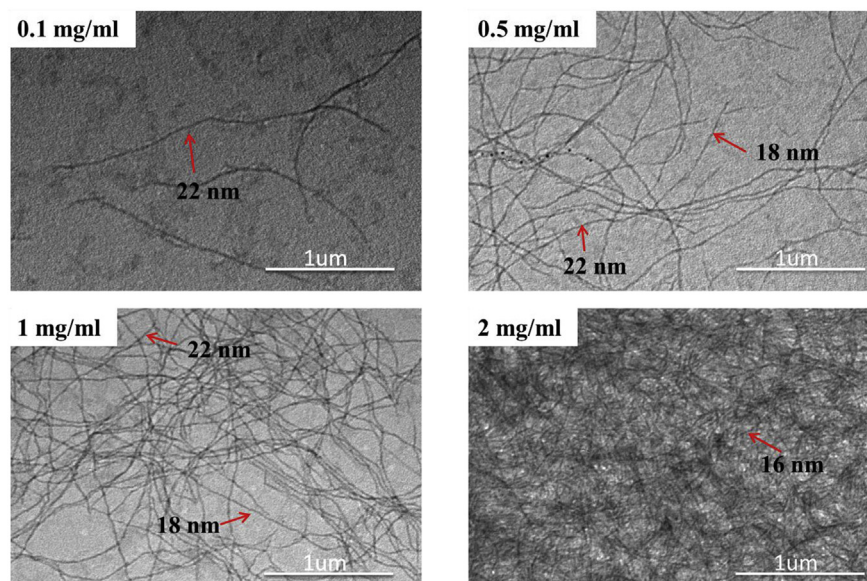
Fig. 6. The morphology of the films drop-casting from the solutions with different concentration.
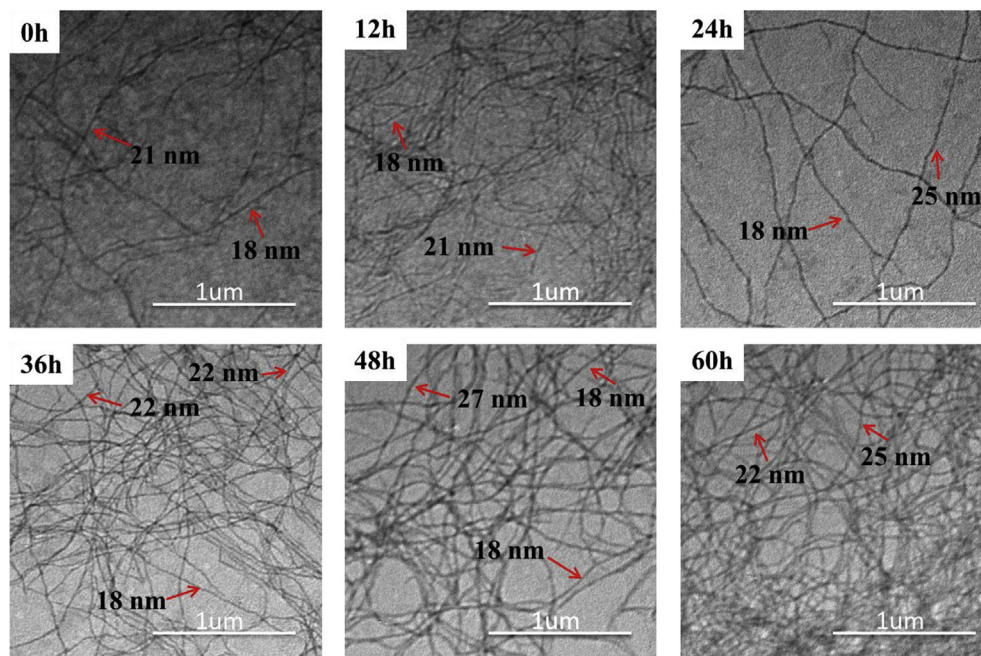
Fig. 8. The morphology of the films drop-casting from the solutions with different aging time.

increased with extending the aging time. The absorption spectra were unchanged at the first 12 h this may be the crystallize nucleation time. The homogeneous nucleation by thermal fluctuations was slow to form perfect nuclei due to the low supersaturation in the solution with small Ra. The amount of aggregation was increased slowly at the next 24 h. The slow aggregation could avoid the defect which was beneficial for forming long nanowires. The intensity of the π-π stacking peak was increased rapidly when the aging time was beyond 36 h and the solution was gelation. This was due to the formed long nanowires were entangled each other and the aggregation was rapidly enhanced. The growing of nanowires in the gelation solution was suppressed. The morphology of the films drop-casting from the solutions aging different time was shown in Fig. 8. There were short nanowires when the solution was aged 0 h and 12 h. The short nanowires were formed during drop-casting process after the crystallize nucleation in solution. The time of forming nanowires during the film formation was shorter than the time of growing nanowires in solution which resulted in the nanowires was short. When the solution was aged 24 h, the nanowires were grown longer which indicated the nanowires were formed in solution. The amount of nanowires was less than the solution aged 12 h which indicated a part of the nucleation was dissolved by thermal fluctuations. When the solution was aged

36 h, the dense nanowires were prepared and the amount of nanowires was increased which indicated the crystallization was a homogeneous nucleation and growth process in solution. The long nanowires were entangled each other when the aging time was beyond 36 h. There was amorphous aggregation at the entanglement apart from nanowires when the solution was aged 48 h and 60 h. The dense and long nanowires were prepared by aging 36 h and the crystallization was a homogeneous nucleation and growth process in solution. The width of nanowires was about 20 nm for different aging time.

The equilibrium of entanglement ↔ disentanglement ↔ nucleation and growth was shown in Fig. 9. The supersaturation in the solution with low Ra and concentration was too small and couldn't crystallize nucleation and growth to form nanowires in solution. The equilibrium was move to the disentanglement. The nanowires formed during the film formation were short and not dense. When the Ra and concentration was increased suitably to the critical value, where the solution is moderately supersaturated, the equilibrium was move to the nucleation and growth. The low supersaturation could drive the conjugated polymer disentangle to adjust conformation for crystallization slowly. The slow crystallize nucleation and growth could form perfect nuclei and reduce defect to prepare the nanowires. The disentangled molecules could pack
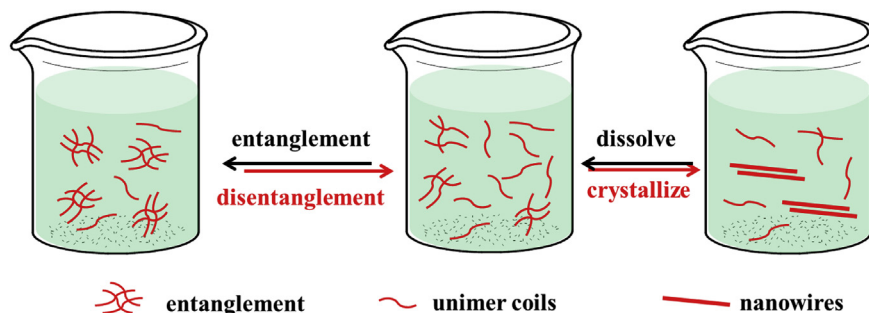
Fig. 9. The equilibrium of entanglement ↔ disentanglement ↔ nucleation and growth.

to nanowires which could facilitate the continuous disentanglement to provide easier diffusivity of chains to grow dense nanowires at higher concentration. The entanglement couldn't be disentangled in the solution with high Ra and concentration which was not beneficial for forming nanowires. The equilibrium was move to the entanglement. The morphology was amorphous aggregation and small crystal. The equilibrium of entanglement ↔ disentanglement ↔ nucleation and growth could be controlled by tuning the Ra. The aging solution with critical Ra at high concentration could form dense and long nanowires.

4. Conclusions

In this work, we control the equilibrium of entanglement ↔ disentanglement ↔ nucleation and growth at higher concentration for the continuous disentanglement with the nucleation and growth of the disentangled molecules. The dense nanowires of PBTTT-C14 were formed by tuning the radius of interaction (Ra) between the solvent and conjugated polymer in the mixed solvent (Ra = 2.56) at a higher concentration of 1 mg/ml by aging. When the solution was at the critical Ra, the entanglement was disentangled at higher concentration. The disentangled molecules could pack to nanowires which could facilitate the continuous disentanglement to grow dense nanowires at higher concentration. The nanowires were more than 10 μm in length and 20 nm in width. The contrast was obvious in transmission electron microscopy which indicated the high electronic density and the high crystallinity of the nanowires. The density of the nanowire increased with increasing concentration and aging time.

Acknowledgements

References

[1] S. Holliday, J.E. Donaghey, I. McCulloch, Advances in charge Carrier mobilities of semiconducting polymers used in organic transistors, Chem. Mater. 26 (1) (2014) 647—663.

[2] Y. Diao, L. Shaw, Z. Bao, S.C.B. Mannsfeld, Morphology control strategies for solution-processed organic semiconductor thin films, Energy Environ. Sci. 7 (7) (2014) 2145—2159.

[3] C.-p. Song, Y. Qu, J.-g. Liu, Y.-c Han, Phase-separation mechanism and morphological control in all-polymer solar cells, Acta Polym. Sin. 2 (2018) 145—163.

[4] C. Wang, H. Dong, L. Jiang, W. Hu, Organic semiconductor crystals, Chem. Soc. Rev. 47 (2) (2018) 422—500.

[5] H. Dong, W. Hu, Multilevel investigation of charge transport in conjugated polymers, Acc. Chem. Res. 49 (11) (2016) 2435—2443.

[6] J.L. Bredas, J.P. Calbert, D.A. da Silva Filho, J. Cornil, Organic semiconductors: a theoretical characterization of the basic parameters governing charge transport, Proc. Natl. Acad. Sci. U. S. A. 99 (9) (2002) 5804—5809.

[7] Y.K. Lan, C.I. Huang, Charge mobility and transport behavior in the ordered and disordered states of the regioregular poly(3-hexylthiophene), J. Phys. Chem. B 113 (44) (2009) 14555—14564.

[8] H.R. Tseng, H. Phan, C. Luo, M. Wang, L.A. Perez, S.N. Patel, L. Ying, E.J. Kramer, T.Q. Nguyen, G.C. Bazan, A.J. Heeger, High-mobility field-effect transistors fabricated with macroscopic aligned semiconducting polymers, Adv. Mater. 26 (19) (2014) 2993—2998.

[9] L. Chen, S. Chi, K. Zhao, J. Liu, X. Yu, Y. Han, Aligned films of the DPP-Based conjugated polymer by solvent vapor enhanced drop casting, Polymer 104 (2016) 123—129.

[10] X. Gao, Y.-c. Han, P3HT stripe structure with oriented nanofibrils enabled by controlled inclining evaporation, Chin. J. Polym. Sci. 31 (4) (2013) 610—619.

[11] X. Gao, R.-b. Xing, J.-g. Liu, Y.-c. Han, Uniaxial alignment of poly(3-hexylthiophene) nanofibers by zone-casting approach, Chin. J. Polym. Sci. 31 (5) (2013) 748—759.

[12] J.H. Kim, D.H. Lee, S. Yang da, D.U. Heo, K.H. Kim, J. Shin, H.J. Kim, K.Y. Baek, K. Lee, H. Baik, M.J. Cho, D.H. Choi, Novel polymer nanowire crystals of diketopyrrolopyrrole-based copolymer with excellent charge transport properties, Adv. Mater. 25 (30) (2013) 4102—4106.

[13] C. Xiao, G. Zhao, A. Zhang, W. Jiang, R.A.J. Janssen, W. Li, W. Hu, Z. Wang, High performance polymer nanowire field-effect transistors with distinct molecular orientations, Adv. Mater. 27 (34) (2015) 4963—4968.

[14] Z.Y. Ma, Y.H. Geng, D.H. Yan, Extended-chain lamellar packing of poly(3-butylthiophene) in single crystals, Polymer 48 (1) (2007) 31—34.

[15] D.H. Kim, J.T. Han, Y.D. Park, Y. Jang, J.H. Cho, M. Hwang, C. Kho, Single-crystal polythiophene microwires grown by self-assembly, Adv. Mater. 18 (6) (2006), 719-+.

[16] K. Rahimi, I. Botiz, N. Stingelin, N. Kayunkid, M. Sommer, F.P.V. Koch, H. Nguyen, O. Coulembier, P. Dubois, M. Brinkmann, G. Reiter, Controllable processes for generating large single crystals of poly(3-hexylthiophene), Angew. Chem. Int. Ed. 51 (44) (2012) 11131—11135.

[17] S. Zenoozi, S. Agbolaghi, H. Gheybi, F. Abbasi, High-quality nano/micro hairy single crystals developed from poly(3-hexylthiophene)-based conductive-dielectric block copolymers having flat-on and edge-on orientations, Macromol. Chem. Phys. 218 (14) (2017), 1700067.

[18] H.A. Um, D.H. Lee, D.U. Heo, D.S. Yang, J. Shin, H. Baik, M.J. Cho, D.H. Choi, High aspect ratio conjugated polymer nanowires for high performance field-effect transistors and phototransistors, ACS Nano 9 (5) (2015) 5264—5274.

[19] W.D. Oosterbaan, V. Vrindts, S. Berson, S. Guillerez, O. Douhéret, B. Ruttens, J. D'Haen, P. Adriaensens, J. Manca, L. Lutsen, D. Vanderzande, Efficient formation, isolation and characterization of poly(3-alkylthiophene) nanofibres: probing order as a function of side-chain length, J. Mater. Chem. 19 (30) (2009) 5424.

[20] L. Janasz, A. Luczak, T. Marszalek, B.G.R. Dupont, J. Jung, J. Ulanski, W. Pisula, Balanced ambipolar organic field-effect transistors by polymer preaggregation, ACS Appl. Mater. Interfaces 9 (24) (2017) 20696—20703.

[21] G.S. Lobov, Y. Zhao, A. Marinins, M. Yan, J. Li, A. Sugunan, L. Thylén, L. Wosinski, M. Östling, M.S. Toprak, S. Popov, Size impact of ordered P3HT nanofibers on optical anisotropy, Macromol. Chem. Phys. 217 (9) (2016) 1089—1095.

[22] X. Cao, Z. Du, L. Chen, K. Zhao, H. Li, J. Liu, Y. Han, Long diketopyrrolopyrrole-based polymer nanowires prepared by decreasing the aggregate speed of the polymer in solution, Polymer 118 (2017) 135—142.

[23] S. Wang, M. Kappl, I. Liebewirth, M. Müller, K. Kirchhoff, W. Pisula, K. Müllen, Organic field-effect transistors based on highly ordered single polymer fibers, Adv. Mater. 24 (3) (2012) 417—420.

[24] Y. Liu, H. Dong, S. Jiang, G. Zhao, Q. Shi, J. Tan, L. Jiang, W. Hu, X. Zhan, High performance nanocrystals of a donor—acceptor conjugated polymer, Chem. Mater. 25 (13) (2013) 2649—2655.

[25] C.-D. Park, T.A. Fleetham, J. Li, B.D. Vogt, High performance bulk-heterojunction organic solar cells fabricated with non-halogenated solvent processing, Org. Electron. 12 (9) (2011) 1465—1470.

[26] M.A. Rogers, A.G. Marangoni, Kinetics of 12-hydroxyoctadecanoic acid SAFiN crystallization rationalized using hansen solubility parameters, Langmuir 32 (48) (2016) 12833—12841.

[27] B. Walker, A. Tamayo, D.T. Duong, X.D. Dang, C. Kim, J. Granstrom, T.Q. Nguyen, A systematic approach to solvent selection based on cohesive energy densities in a molecular bulk heterojunction system, Adv. Energy Mater. 1 (2) (2011) 221—229.

[28] C.E. Johnson, D.S. Boucher, Poly(3-hexylthiophene) aggregate formation in binary solvent mixtures: an excitonic coupling analysis, J. Polym. Sci., Part B: Polym. Phys. 52 (7) (2014) 526—538.

[29] C.E. Johnson, M.P. Gordon, D.S. Boucher, Rationalizing the self-assembly of poly-(3-hexylthiophene) using solubility and solvatochromic parameters, J. Polym. Sci., Part B: Polym. Phys. 53 (12) (2015) 841—850.

[30] Y. Lan, M.G. Corradini, X. Liu, T.E. May, F. Borondics, R.G. Weiss, M.A. Rogers, Comparing and correlating solubility parameters governing the self-assembly of molecular gels using 1,3:2,4-dibenzylidene sorbitol as the gelator, Langmuir 30 (47) (2014) 14128—14142.

[31] I. Burgués-Ceballos, F. Machui, J. Min, T. Ameri, M.M. Voigt, Y.N. Luponosov, S.A. Ponomarenko, P.D. Lacharmoise, M. Campoy-Quiles, C.J. Brabec, Solubility based identification of green solvents for small molecule organic solar cells, Adv. Funct. Mater. 24 (10) (2014) 1449—1457.

[32] W.-Y. Lee, G. Giri, Y. Diao, C.J. Tassone, J.R. Matthews, M.L. Sorensen, S.C.B. Mannsfeld, W.-C. Chen, H.H. Fong, J.B.H. Tok, M.F. Toney, M. He, Z. Bao, Effect of non-chlorinated mixed solvents on charge transport and morphology of solution-processed polymer field-effect transistors, Adv. Funct. Mater. 24 (23) (2014) 3524—3534.

[33] H.L. Yi, C.H. Wu, C.I. Wang, C.C. Hua, Solvent-regulated mesoscale aggregation properties of dilute PBTTT-C14 solutions, Macromolecules 50 (14) (2017) 5498—5509.

[34] R.J. Kline, M.D. McGehee, E.N. Kadnikova, J.S. Liu, J.M.J. Frechet, M.F. Toney, Dependence of regioregular poly(3-hexylthiophene) film morphology and field-effect mobility on molecular weight, Macromolecules 38 (8) (2005) 3312—3319.

[35] X. Yuan, W. Zhang, L.H. Xie, J. Ma, W. Huang, W. Liu, Role of planar conformations in aggregation induced spectral shifts of supermolecular oligo-fluorenols in solutions and films: a combined experimental and MD/TD-DFT study, J. Phys. Chem. B 119 (32) (2015) 10316—10333.

[36] T.J. Fauvell, T. Zheng, N.E. Jackson, M.A. Ratner, L. Yu, L.X. Chen, Photophysical and morphological implications of single-strand conjugated polymer folding in solution, Chem. Mater. 28 (8) (2016) 2814—2822.